J Electroceram (2006) 17:1069–1073
DOI 10.1007/s10832-006-8317-6

Effect of Cr_2O_3 addition on the microstructure and electrical properties of Mn-Ni-Co oxides NTC thermistors

K. Park · I. H. Han

Received: 30 June 2005 / Revised: 8 March 2006 / Accepted: 16 March 2006

Abstract The as-sintered $Mn_{1.1}Ni_{1.4}Co_{0.5}O_4$ crystallized in the solid solution of cubic spinel Mn-Ni-Co oxides, along with a small amount of the cubic spinel Ni-rich oxide phase. On the other hand, the Cr-substituted $Mn_{1.1}Ni_{1.4}Co_{0.5-x}Cr_xO_4$ ($0.07 \leqq x \leqq 0.35$) showed a single phase of cubic spinel Mn-Ni-Co-Cr oxides. This indicates that the substituted Cr suppressed the decomposition in the oxides. In addition, the Cr hindered the grain growth during sintering and increased the porosity. The electrical resistivity, the $B_{25/85}$ constant, and the activation energy of the $Mn_{1.1}Ni_{1.4}Co_{0.5-x}Cr_xO_4$ NTC thermistors increased with increasing Cr content. It is demonstrated that the Cr-substituted $Mn_{1.1}Ni_{1.4}Co_{0.5-x}Cr_xO_4$ NTC thermistors provided a variety of electrical properties, depending on the composition.

Keywords $Mn_{1.1}Ni_{1.4}Co_{0.5-x}Cr_xO_4$ · Microstructure · Electrical resistivity · NTC thermistor · Spinel structure

1 Introduction

Transition metal manganites $Mn_{3-x}M_xO_4$ (M = Ni, Cu, Fe, Co, etc) are technologically important materials used as negative temperature coefficient (NTC) thermistor materials owing to their interesting electrical properties [1]. Their electrical resistivity ρ varies exponentially with temperature T by the well known Arrhenius equation $\rho = \rho_o \exp(B/T)$ [1], where ρ_o is the resistivity of the material at infinite temperature and B is the B constant, which is a measure of the sensitivity of the device over a given temperature. Here, the B constant has the dimensions of the absolute temperature and is given by the following equation: $B = E_a/k_B$, where E_a is the activation energy for electrical conduction and k_B is the Boltzmann constant. The activation energy is primarily the energy for the hopping process from a cation M^{n+} to $M^{(n+1)+}$ on the octahedral sites and, hence, for the mobility of the cations [2–4]. The B constant can be calculated by the following equation [1]: $B = (\ln\rho_1 - \ln\rho_2)/(1/T_1 - 1/T_2)$, where ρ_1 and ρ_2 are the resistivities measured at temperatures T_1 and T_2, respectively.

The oxides typically exhibit the spinel-type crystal structure with the general formula AB_2O_4 [5, 6]. The selection of a given metal oxide material for the applications of NTC thermistors is mainly determined by the required resistivity and the $B_{25/85}$ constant, i.e., the thermal sensitivity. In general, the electrical properties depend on the composition, which strongly influences the distribution of cations in the spinel structure [7–9]. In the present study, we investigated the microstructure and electrical properties of the $Mn_{1.1}Ni_{1.4}Co_{0.5-x}Cr_xO_4$ ($0 \leqq x \leqq 0.35$) NTC thermistors fabricated by the solid-state reaction method, especially with regard to the partial substitution of Cr for Co.

2 Experimental

High-purity Mn_3O_4, NiO, Co_3O_4, and Cr_2O_3 powders were weighed in appropriate proportions to fabricate $Mn_{1.1}Ni_{1.4}Co_{0.5-x}Cr_xO_4$ ($x = 0$, 0.07, 0.14, 0.21, 0.28, and 0.35). The mixture of weighed powders and distilled water was milled for 6 h using a planetary mill (FRITSCH pulverisette 6) and ZrO_2 as grinding media. The resulting slurries were dried at 80°C in an oven for 24 h. Thermal analysis of the oxide mixture was carried out using a differential thermal/thermogravimetric analysis (DT/TGA) (SCINCO

K. Park (✉)· I.H. Han
Department of Advanced Materials Engineering, Sejong University, Seoul 143-747, Korea
e-mail: kspark@sejong.ac.kr

Co. STA S-1500) in the temperature range of 0 to 1200°C at a heating rate of 10°C min^{-1} in air. The granulated powders were calcined in a mullite crucible at 950°C for 2 h. Subsequently, the mixture of powders was pressed using a hand press at a pressure of 98 MPa to prepare pellets of 1 mm-thick and 8-mm in diameter. The green compacts were heated at 1260°C for 3 h in air and then furnace cooled.

The crystalline structure of the as-sintered $Mn_{1.1}Ni_{1.4}Co_{0.5-x}Cr_xO_4$ samples was analyzed with X-ray diffraction (XRD) (Rigaku DMAX 2500) using Cu Kα radiation at 40 kV and 25 mA. The microstructure of the samples was investigated by a scanning electron microscope (SEM) (Hitachi S4200). The Ag paste with a thickness of $\sim$15 μm was spread on opposite-side surfaces of the sintered samples using a screen printer. After the paste was dried at room temperature, the samples were heated at 850°C for 10 min. The samples were held with a holder in a bath of silicone oil, and their temperatures were measured with a digital thermometer. The electrical resistance was measured with a digital multimeter (Fluke 45) from 25°C up to 115°C in steps of 10°C.

3 Results and discussion

Figures 1(a) and (b) show the results of the DTA and TGA measurements for a mixture of the oxide powders of $Mn_{1.1}Ni_{1.4}Co_{0.5}O_4$ and $Mn_{1.1}Ni_{1.4}Co_{0.22}Cr_{0.28}O_4$ samples, respectively. The weight loss of $\sim$0.19% in region I, accompanied with the exothermic reaction, is due to the removal of absorbed water and organic volatiles present in the samples [10]. Subsequently, several oxido-reduction phenomena are observed for the two samples [11, 12]. A slight weight gain in region II is attributed to the oxidation of Mn^{3+} cations on octahedral sites. When the temperature is further increased (region III), a weight significantly increased because of the oxidation of the tetrahedral Mn^{2+}. For higher temperatures (region IV), the powders start to lose weight. This is due to the reduction of Mn^{4+} to Mn^{3+} ions. Finally, for temperatures higher than region IV (region V), we can find a significant weight loss of the powders, which is associated with the reduction of Mn^{3+} ions and the loss of excess oxygen, and the stoichiometry of the sample is progressively restored.

Figures 2(a) and (b) show SEM images obtained from the surface of the as-sintered $Mn_{1.1}Ni_{1.4}Co_{0.5}O_4$ and $Mn_{1.1}Ni_{1.4}Co_{0.22}Cr_{0.28}O_4$ samples, respectively. The mean grain sizes of the $Mn_{1.1}Ni_{1.4}Co_{0.5}O_4$ and $Mn_{1.1}Ni_{1.4}Co_{0.22}Cr_{0.28}O_4$ samples were 5.2 and 3.1 μm, respectively, indicating that the substituted Cr hindered the grain growth during sintering. This is caused by the dragging effect between the added Cr_2O_3 and the grain boundaries, which retards the grain growth [13]. It was also observed that the $Mn_{1.1}Ni_{1.4}Co_{0.5-x}Cr_xO_4$ ($0 \leqq x \leqq 0.35$) samples were

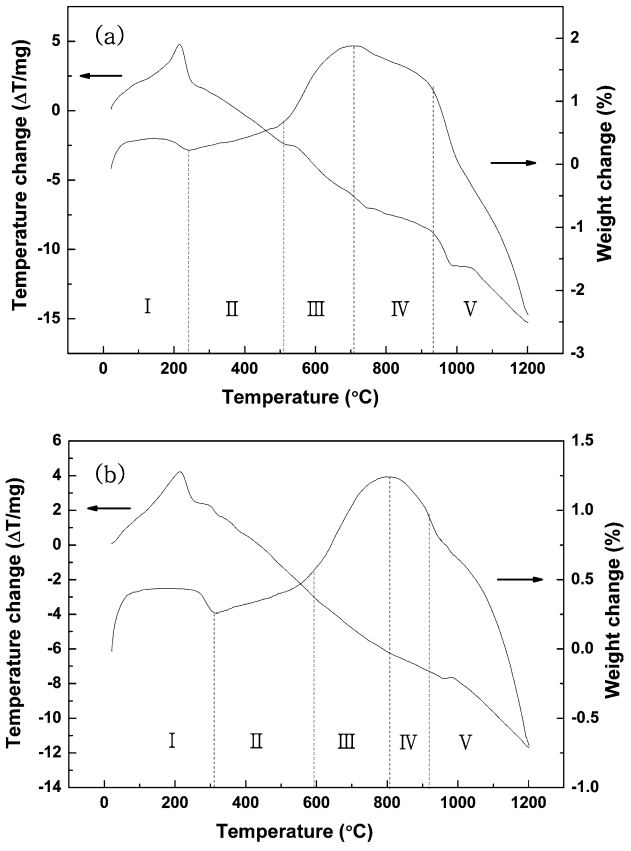

Fig. 1 Results of the DTA and TGA measurements for a mixture of the oxide powders of (a) $Mn_{1.1}Ni_{1.4}Co_{0.5}O_4$ and (b) $Mn_{1.1}Ni_{1.4}Co_{0.22}Cr_{0.28}O_4$ samples

highly dense. The relative density of the samples decreased with an increase in Cr content, ranging from 98 to 95% of the theoretical density. A dense microstructure is necessary to obtain a good reproducibility of the electrical characteristics of the ceramics.

It was found that the as-sintered $Mn_{1.1}Ni_{1.4}Co_{0.5}O_4$ crystallized in the solid solution of Mn-Ni-Co oxides with a cubic spinel structure, along with a small amount of the cubic spinel Ni-rich oxide phase. The Ni-rich oxide phase was formed by the decomposition in the solid solution [14]. This result for the decomposition is in good agreement with that reported by previous workers [2, 15, 16]. They investigated the dependence of oxygen release on the temperature of the decomposition. It is closely associated with the loss of oxygen in the ceramics during sintering. On the other hand, the Cr-substituted $Mn_{1.1}Ni_{1.4}Co_{0.5-x}Cr_xO_4$ ($0.07 \leqq x \leqq 0.35$) showed a single phase of cubic spinel Mn-Ni-Co-Cr oxides, suggesting that the substituted Cr suppressed a loss and transportation of oxygen. The substituted Cr did not affect the crystalline structure and formed a solid solution with Mn-Ni-Co oxides.

In particular, as the Cr content increased, the XRD peaks of the Cr-substituted $Mn_{1.1}Ni_{1.4}Co_{0.5-x}Cr_xO_4$ ($0.07 \leqq x \leqq$

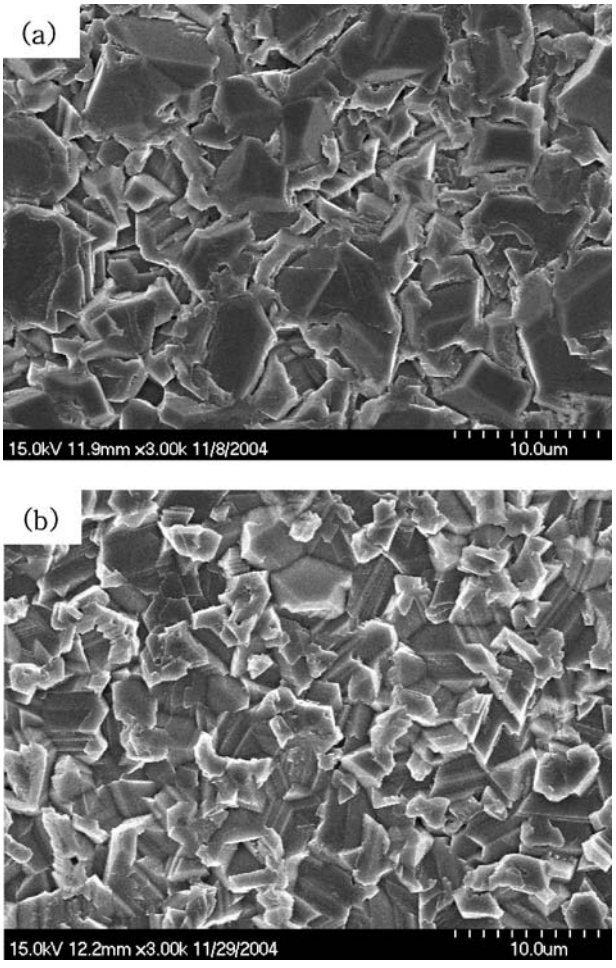

Fig. 2 SEM images obtained from the surface of as-sintered (a) $Mn_{1.1}Ni_{1.4}Co_{0.5}O_4$ and (b) $Mn_{1.1}Ni_{1.4}Co_{0.22}Cr_{0.28}O_4$ samples

0.35) samples shifte slightly towards higher angles with respect to the cubic spinel Mn-Ni-Co oxide phase of $Mn_{1.1}Ni_{1.4}Co_{0.5}O_4$ sample, indicating that the lattice parameter slightly decreased with an increase in Cr content. The results obtained for the lattice parameter of the $Mn_{1.1}Ni_{1.4}Co_{0.5-x}Cr_xO_4$ ($0 \leqq x \leqq 0.35$) samples are summarized in Table 1. The standard error on lattice parameter was less than ± 0.005 Å. It is believed that the substituted Cr

Table 1 Variation of the lattice parameter of $Mn_{1.1}Ni_{1.4}Co_{0.5-x}Cr_xO_4$ ($0 \leqq x \leqq 0.35$) samples

Sample	Lattice parameter (Å)
$Mn_{1.1}Ni_{1.4}Co_{0.5}O_4$	8.3554
$Mn_{1.1}Ni_{1.4}Co_{0.43}Cr_{0.07}O_4$	8.3404
$Mn_{1.1}Ni_{1.4}Co_{0.36}Cr_{0.14}O_4$	8.3343
$Mn_{1.1}Ni_{1.4}Co_{0.29}Cr_{0.21}O_4$	8.3318
$Mn_{1.1}Ni_{1.4}Co_{0.22}Cr_{0.28}O_4$	8.3299
$Mn_{1.1}Ni_{1.4}Co_{0.15}Cr_{0.35}O_4$	8.3289

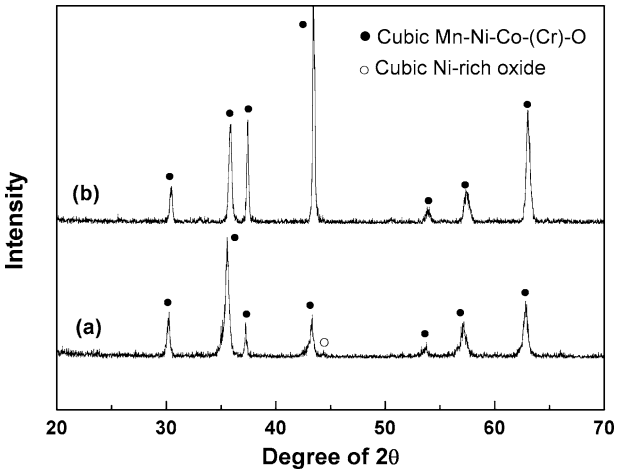

Fig. 3 XRD patterns of as-sintered (a) $Mn_{1.1}Ni_{1.4}Co_{0.5}O_4$ and (b) $Mn_{1.1}Ni_{1.4}Co_{0.29}Cr_{0.21}O_4$ samples

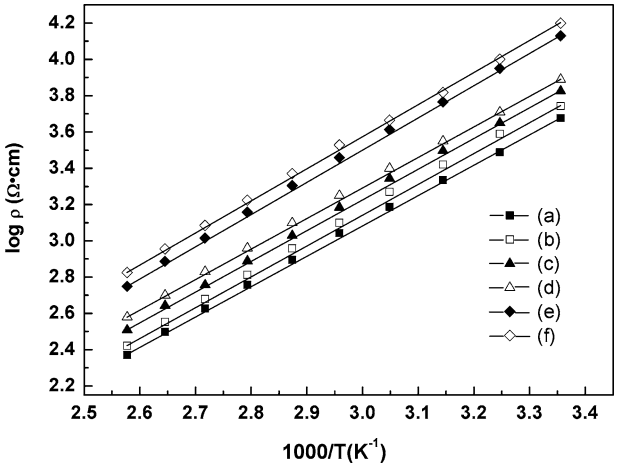

Fig. 4 A plot of log ρ against the reciprocal of the absolute temperature ($1/T$) for (a) $Mn_{1.1}Ni_{1.4}Co_{0.5}O_4$, (b) $Mn_{1.1}Ni_{1.4}Co_{0.43}Cr_{0.07}O_4$, (c) $Mn_{1.1}Ni_{1.4}Co_{0.36}Cr_{0.14}O_4$, (d) $Mn_{1.1}Ni_{1.4}Co_{0.29}Cr_{0.21}O_4$, (e) $Mn_{1.1}Ni_{1.4}Co_{0.22}Cr_{0.28}O_4$, and (f) $Mn_{1.1}Ni_{1.4}Co_{0.15}Cr_{0.35}O_4$ NTC thermistors

is present on substitutional sites in the cubic spinel lattice to form substitutional solid solution. The ionic crystal radii of Co^{2+} and Cr^{2+} are 0.74 and 0.73 Å, respectively [17]. For example, the XRD patterns of the $Mn_{1.1}Ni_{1.4}Co_{0.5}O_4$ and $Mn_{1.1}Ni_{1.4}Co_{0.29}Cr_{0.21}O_4$ samples are shown in Figs. 3(a) and (b), respectively. No peaks corresponding to the Ni-rich oxide phase were detected in the $Mn_{1.1}Ni_{1.4}Co_{0.29}Cr_{0.21}O_4$ sample, indicating that the substituted Cr suppressed the decomposition in the solid solution.

Figure 4 shows a plot of log ρ against the reciprocal of the absolute temperature ($1/T$) for the $Mn_{1.1}Ni_{1.4}Co_{0.5-x}Cr_xO_4$ ($0 \leqq x \leqq 0.35$) NTC thermistors. This figure reveals a nearly linear dependence of log ρ versus 1/T in the range of temperature measured, indicating semiconducting NTC thermistor characteristics. The slope of the log ρ versus 1/T curve is taken generally as a measure of the activation energy of

Table 2 Resistivity at 25 and 85°C, $B_{25/85}$ constant, and activation energy of the prepared $Mn_{1.1}Ni_{1.4}Co_{0.5-x}Cr_xO_4$ ($0 \leqq x \leqq 0.35$) NTC thermistors

Sample	Resistivity at 25°C (Ω·cm)	Resistivity at 85°C (Ω·cm)	$B_{25/85}$ constant (K)	Activation energy (eV)
$Mn_{1.1}Ni_{1.4}Co_{0.5}O_4$	4753	573	2386	0.206
$Mn_{1.1}Ni_{1.4}Co_{0.43}Cr_{0.07}O_4$	5534	649	2642	0.228
$Mn_{1.1}Ni_{1.4}Co_{0.36}Cr_{0.14}O_4$	6691	774	3014	0.260
$Mn_{1.1}Ni_{1.4}Co_{0.29}Cr_{0.21}O_4$	7762	912	3264	0.281
$Mn_{1.1}Ni_{1.4}Co_{0.22}Cr_{0.28}O_4$	13490	1438	4242	0.365
$Mn_{1.1}Ni_{1.4}Co_{0.15}Cr_{0.35}O_4$	15849	1677	4492	0.387

conductivity. Also, the sensitivity index, the $B_{25/85}$ constant, is calculated from this figure. The calculated activation energy and $B_{25/85}$ constant of the $Mn_{1.1}Ni_{1.4}Co_{0.5-x}Cr_xO_4$ NTC thermistors are listed in Table 2, together with the resistivity at 25 and 85°C. The values of ρ_{25}, ρ_{85}, the $B_{25/85}$ constant, and the activation energy of the NTC thermistors with different compositions are 4753–15849 Ωcm, 573–1677 Ωcm, 2386–4492 K, and 0.206–0.387 eV, respectively. This indicates that the electrical properties of the NTC thermistors can be controlled by changing the composition.

We found that the resistivity of the thermistors increased as the Cr content increased. There are two possible reasons for the increase in the resistivity with increasing Cr content. (1) As discussed previously, both the grain size and density of the as-sintered samples decreased with an increase in Cr content, decreasing the time between electron scattering events of charge carriers and thus increasing the resistivity. (2) The amount of Co_3O_4 for the thermistors decreases with increasing Cr content, decreasing Co^{2+}/Co^{3+} ions on octahedral sites. As a result, the number of Mn^{3+}/Mn^{4+} ions on octahedral sites decreases to preserve the overall electrical neutrality of the system. It is also clear that the $B_{25/85}$ constant progressively increased with increasing Cr content, indicating that the thermistor sensitivity improved. For practical applications, a more higher value of the $B_{25/85}$ constant is desirable because the resistivity is more sensitive to variation of temperature, providing more accurate and smaller variations in temperature measurements. In addition, the activation energy of the thermistors increased with increasing Cr content. The activation energy is the energy for the hopping of electrons between the Mn^{3+} and Mn^{4+} ions on octahedral sites [18–20].

On the basis of the above results, the values of measured electrical properties satisfy the requirements for being used as industrial NTC thermistors. Generally, the values of the $B_{25/85}$ constant and the activation energy of the thermistors are 2000–7000 K and 0.1–1.5 eV, respectively [21]. The values of the resistivity and the $B_{25/85}$ constant are adjustable to desired values, depending on the composition. It is thus concluded that the partial substitution of Cr for Co in $Mn_{1.1}Ni_{1.4}Co_{0.5}O_4$ is desirable for a wide range of practical applications of the NTC thermistors.

4 Conclusions

The crystal structure of the as-sintered $Mn_{1.1}Ni_{1.4}Co_{0.5}O_4$ was the solid solution of Mn-Ni-Co oxides with a cubic spinel structure, along with a small amount of the cubic spinel Ni-rich oxide phase, indicating a decomposition of the Ni-rich oxide phase in the solid solution. The phase decomposition was likely to occur with the loss of oxygen in the ceramics during sintering. On the other hand, the Cr-substituted $Mn_{1.1}Ni_{1.4}Co_{0.5-x}Cr_xO_4$ ($0.07 \leqq x \leqq 0.35$) showed a single phase of cubic spinel Mn-Ni-Co-Cr oxides. No Ni-rich phase was detected in the Cr-substituted samples, indicating that the substituted Cr suppressed the decomposition in the oxides. The substituted Cr did not affect the crystalline structure and formed a solid solution with Mn-Ni-Co oxides. The grain size and density of the $Mn_{1.1}Ni_{1.4}Co_{0.5-x}Cr_xO_4$ samples decreased with an increase in Cr content. The values of ρ_{25}, ρ_{85}, $B_{25/85}$ constant, and the activation energy of the NTC thermistors were 4753–15849 Ω·cm, 573–1677 Ω·cm, 2386–4492 K, and 0.206–0.387 eV, respectively. In particular, the substituted Cr led to an increase in both the resistivity and the sensitivity index, the $B_{25/85}$ constant. It is concluded that the Cr substituted $Mn_{1.1}Ni_{1.4}Co_{0.5-x}Cr_xO_4$ ceramics are useful for industrial applications as NTC thermistors over a wide temperature range.

References

1. E.D. Macklen, *Thermistors* (Electrochemical Publications Ltd., Ayr, Scotland, 1979), pp. 1–33.
2. E.D. Macklen, *J. Phys. Chem. Solids*, **47**, 1073 (1986).
3. A. Feltz, J. Töpfer, and F. Schirrmeister, *J. Eur. Ceram. Soc.*, **9**, 187 (1992).
4. S.E. Dorris and T.O. Mason, *J. Am. Ceram. Soc.*, **71**, 379 (1988).
5. E.G. Larson, R.J. Arnott, and D.G. Wickham, *J. Phys. Chem. Solids*, **23**, 1771 (1962).

6. V.A.M. Brabers, F.M.V. Setten, and P.S.A. Knapen, *J. Solid State Chem.*, **49**, 93 (1983).
7. S.K. Sarkar, M.L. Sharma, H.L. Bhaskar, and K.C. Nagpal, *J. Mater. Sci.*, **19**, 545 (1984).
8. S.L. Fu and I.C. Ho, *J. Mater. Sci. Lett.*, **8**, 999 (1989).
9. R. Metz, J.P. Caffin, R. Legros, and A. Rousset, *J. Mater. Sci.*, **24**, 83 (1989).
10. N. Torikai, T. Meguro, T. Sasamoto, H. Nakayama, T. Yokoyama, and Y. Abe, *J. Chem. Soc. Japan*, 785 (1984).
11. S. Guillemet-Fritsch, J. Salmi, J. Sarrias, A. Rousset, S. Schuurman, and A. Lannoo, *Mater. Res. Bull.*, **39**, 1957 (2004).
12. B. Gillot, M.E. Guendouzi, M. Kharroubi, P. Tailhades, R. Metz, and A. Rousset, *Mater. Chem. Phys.*, **24**, 199 (1989).
13. S.J. Bennison and M.P. Harmer, *J. Am. Ceram. Soc.*, **68**, C22 (1985).
14. T. Meguro, T. Sasamoto, T. Yokoyama, S. Yamada, Y. Abe, and N. Torikai, *J. Japanese Ceram. Soc.*, **95**, 336 (1987).
15. J. Jung, J. Töpfer, J. Mürbe, and A. Feltz, *J. Eur. Ceram. Soc.*, **6**, 351 (1990).
16. G.D.C. Csete de Györgyfalva, A.N. Nolte, and I.M. Reaney, *J. Eur. Ceram. Soc.*, **21**, 2145 (2001).
17. W.D. Kingery, H.K. Bowen, and D.R. Uhlmann, *Introduction to Ceramics* (John Wiley and Sons, Inc., New York, 1976), p. 58.
18. T. Battault, R. Legros, and A. Rousset, *J. Eur. Ceram. Soc.*, **15**, 1141 (1995).
19. H.J. Van Daal and A.J. Bosman, *Phys. Rev.*, **158**, 736 (1967).
20. I.G. Austin and N.F. Mott, *Adv. Phys.*, **18**, 41 (1969).
21. J.L. Martin de Vidales, P. Garcia-Chain, R.M. Rojas, E. Vila, and O. Garcia-Martinez, *J. Mater. Sci.*, **33**, 1491 (1998).